

Out-of-time-order correlations and the fine structure of eigenstate thermalisation

Marlon Brenes,^{1,*} Silvia Pappalardi,^{2,†} Mark T. Mitchison,¹ John Goold,¹ and Alessandro Silva³

¹*Department of Physics, Trinity College Dublin, Dublin 2, Ireland*

²*Laboratoire de Physique de l'École Normale Supérieure, Paris, France*

³*SISSA, Via Bonomea 265, I-34135 Trieste, Italy*

(Dated: May 29, 2022)

Out-of-time-order correlators (OTOCs) have become established as a tool to characterise quantum information dynamics and thermalisation in interacting quantum many-body systems. It was recently argued that the expected exponential growth of the OTOC is connected to the existence of correlations beyond those encoded in the standard Eigenstate Thermalisation Hypothesis (ETH). We show explicitly, by an extensive numerical analysis of the statistics of operator matrix elements in conjunction with a detailed study of OTOC dynamics, that the OTOC is indeed a precise tool to explore the fine details of the ETH. In particular, while short-time dynamics is dominated by correlations, the long-time saturation behaviour gives clear indications of an operator-dependent energy scale associated to the emergence of an effective Gaussian random matrix theory.

Introduction.—Understanding how isolated quantum systems thermalise under unitary evolution is a theme as old as quantum mechanics itself [1, 2]. This line of study has seen significant renewed interest in the past decades [3–7] primarily due to spectacular advances in ultra-cold atom physics [8–10] which have allowed the observation of coherent dynamics over long times.

In isolated classical systems, thermalisation relies on the emergence of chaos and ergodicity, which together lead phase-space trajectories starting from the same energy to become indistinguishable when averaged over time [11]. The equivalent notion of indistinguishability in quantum many-body systems is provided by the Eigenstate Thermalisation Hypothesis (ETH) [7, 12, 13], which states that nearby energy eigenstates cannot be distinguished by local observations. More precisely, the ETH requires the matrix elements of few-body observables in the eigenbasis of a many-body Hamiltonian to obey the following ansatz, which implies thermalisation [7, 14]:

$$O_{nm} = O(\bar{E})\delta_{nm} + e^{-S(\bar{E})/2} f_{\bar{O}}(\bar{E}, \omega) R_{nm}. \quad (1)$$

Here, both $O(\bar{E})$ and $f_{\bar{O}}(\bar{E}, \omega)$ are smooth functions of their arguments $\bar{E} = (E_n + E_m)/2$ and $\omega = E_m - E_n$, $S(\bar{E})$ is the microcanonical entropy, and R_{nm} is a pseudo-random *statistical matrix* with zero average and unit variance.

More recently, thermalization has been explored from a new quantum information perspective, with emphasis on the notion of scrambling [15]. Information scrambling is a more primordial feature of quantum dynamical systems where information, initially stored locally, gets dynamically distributed in global degrees of freedom [16]. This process is explained as a consequence of the growth of operator complexity under time evolution [17]. Although traditional tools can hardly be of any help in studying this phenomenon, a variety of ideas have emerged recently for this task. Among them, the out-of-time-order correlator (OTOC) [18], suggested to characterise synthetic analogues of black-holes [19–21],

has arisen as an important figure of merit for scrambling, ergodicity and quantum chaos in complex many-body quantum systems. Several experimental studies with a variety of platforms have demonstrated that OTOCs indeed characterise scrambling following the operation of a unitary circuit [22–25].

Recently, Foini and Kurchan [26] argued that, in order for the expected exponential growth rate of OTOCs in chaotic models [21] to be positive, correlations between the matrix elements of operators in the energy eigenbasis must exist and thus they generalised the standard ETH in Eq. (1) to account for such correlations. Based on this result, Murthy and Srednicki [27] were able to derive known bounds on the growth rate from the ETH. Chan et al. [28] showed that in locally interacting systems the butterfly effect for OTOCs implies a universal form for these correlations. The existence of frequency-dependent correlations has recently been confirmed by Richter et al. [29] by a numerical investigation of the statistical distributions of matrix elements in non-integrable systems. Despite all of this progress, however, a systematic study of the properties of the statistical matrix in conjunction with OTOCs for realistic models is presently lacking.

Here, we fill this gap by an extensive study of the frequency and energy dependence of the statistics of off-diagonal matrix elements and of the OTOCs of selected observables in two experimentally relevant models: hardcore bosons with dipolar interactions in a harmonic trap [30] and an Ising chain with longitudinal and transverse fields [31]. In all instances, the statistical matrix appears to have some common features. The matrix elements R_{nm} at a given energy \bar{E} and frequency ω obey Gaussian statistics [29, 32–38], in contrast with non-ergodic systems [38–41]. We demonstrate that this feature persists well beyond the infinite-temperature limit. We also find the existence of statistical correlations between R_{nm} at well-separated frequencies. However, these correlations disappear between matrix elements close to the diagonal, indicating the emergence of random-matrix-like behaviour at small frequencies $|E_n - E_m| < \omega_{\text{GOE}}$ [29], where ω_{GOE} is a model-

and operator-dependent energy scale. We show explicitly that this rich structure is naturally reflected in the dynamics of OTOCs. A comparison between the OTOCs computed on a thermal ensemble and those computed assuming the ETH with a random Gaussian statistical matrix shows convergence of the two on time scales that appear to be related to ω_{GOE}^{-1} . This suggests that an experimental study of OTOCs could be an efficient way to probe the energy scales beyond which a complex, interacting system displays Gaussian random-matrix behaviour in local observables.

Models and observables.—In order to address the generic behaviour of thermalising systems that is independent of microscopic details, we consider two different non-integrable models: the first describing hard-core bosons with dipolar interactions in a harmonic trap [30], while the second is a quantum Ising chain with both transverse and longitudinal fields [31]. The microscopic Hamiltonian of the first model is ($\hbar := 1$)

$$\hat{H}_{\text{HB}} = \sum_{i=1}^{L-1} J \left(\hat{b}_i^\dagger \hat{b}_{i+1} + \text{H.c.} \right) + \sum_{i < l} \frac{V \hat{n}_i \hat{n}_l}{|i-l|^3} + \sum_i g x_i^2 \hat{n}_i, \quad (2)$$

for a one-dimensional chain with L sites where \hat{b}_i^\dagger and \hat{b}_i are hard-core bosonic creation and annihilation operators, respectively, at site i , $\hat{n}_i = \hat{b}_i^\dagger \hat{b}_i$, and $x_i = |i - L/2|$. Hereafter, all energies are given in units of the hopping amplitude J and we set the strength of the dipolar interaction and confining potential to be $V = 2$ and $g = 16/(L-1)^2$, respectively (parameters selected from Ref. [30]). Since the system conserves the total number of bosons, we focus on the half-filled subsector, in which the Hilbert space dimension is $\mathcal{D} = L! / [(L/2)!(L/2)!]$. To avoid parity (spatial inversion) or reflection (spin inversion) symmetries, we add a small perturbation $\delta \hat{n}_1$ to the Hamiltonian ($\delta = 0.1J$).

The second model has the following Hamiltonian:

$$\hat{H}_{\text{IS}} = \sum_{i=1}^L w \hat{\sigma}_i^x + \sum_{i=1}^L h \hat{\sigma}_i^z + \sum_{i=1}^{L-1} J \hat{\sigma}_i^z \hat{\sigma}_{i+1}^z. \quad (3)$$

We measure energies in units J and set $w = \sqrt{5}/2$, $h = (\sqrt{5} + 5)/8$ (see [31]). We consider the even parity subsector for chains with an even number of sites, with a corresponding Hilbert space dimension $\mathcal{D} = 2^L - [(2^L - 2^{L/2})/2]$.

We consider few-body observables, which can be either local such as

$$\hat{A}_{\text{HB}} = \hat{n}_{\frac{L}{2}} \hat{n}_{\frac{L}{2}+1}, \quad \hat{A}_{\text{IS}} = \hat{\sigma}_{\frac{L}{2}}^z \hat{\sigma}_{\frac{L}{2}+1}^z, \quad (4)$$

or extensive sums of local operators spanning the entire system:

$$\hat{B}_{\text{HB}} = \frac{1}{L} \sum_i [1 + (-1)^i] \hat{n}_i, \quad \hat{B}_{\text{IS}} = \frac{1}{L} \sum_i \hat{\sigma}_i^z. \quad (5)$$

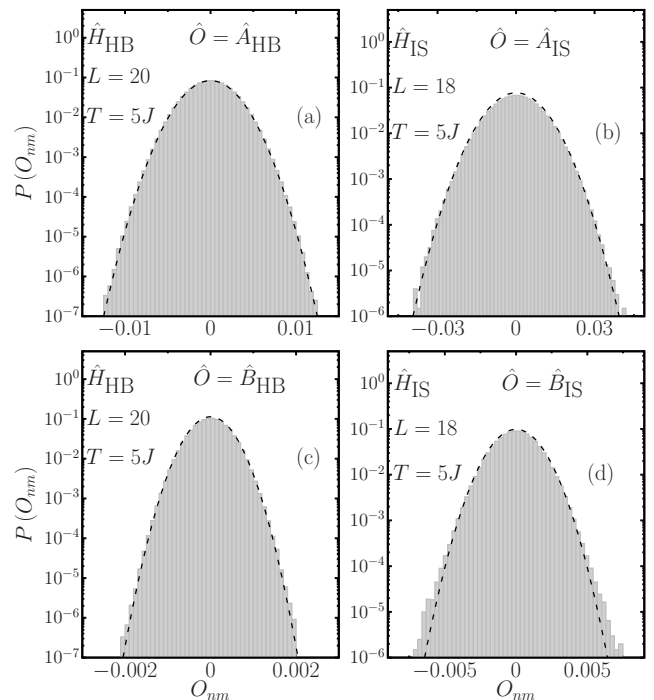


FIG. 1. Probability distributions of off-diagonal matrix elements in a small frequency range $\omega \lesssim 0.05$. The average energy \bar{E} selected is consistent with a finite canonical temperature $T = 5J$. The distributions for local operators are shown in (a) for \hat{A}_{HB} and in (b) for \hat{A}_{IS} . The corresponding distributions for sums of local operators are shown in (c) for \hat{B}_{HB} and in (d) for \hat{B}_{IS} . Results obtained for finite-sized systems of $L = 20$ for \hat{H}_{HB} and $L = 18$ for \hat{H}_{IS} . Dashed lines depict a Gaussian with the same mean and variance.

A detailed study of the diagonal matrix elements and two-point correlation functions of these operators demonstrates the validity of the ETH in both models [42].

It is crucial to recognise that, within the ETH formalism, the one- and two-point correlation functions do not depend on the details of the statistical matrix R_{nm} . In particular, two-point correlators are determined by the smooth function $f_{\hat{O}}(\bar{E}, \omega)$ entering Eq. (1), which itself depends only on the variance of matrix elements O_{nm} near a given energy \bar{E} and frequency ω [30, 32, 35, 38, 43–45]. The precise distribution of these elements, as well as correlations between matrix elements at different frequencies, thus encode the fine structure of the ETH beyond linear-response theory [26]. In the following, we investigate how this structure influences the dynamics of higher-order correlators such as the OTOC.

Gaussian statistics.—The first step towards a statistical characterisation of \hat{O} is to understand the distribution of its individual matrix elements. Since the number of matrix elements is very large even at small system sizes, we begin by studying the distribution of off-diagonal matrix elements $O_{nm} = \langle E_n | \hat{O} | E_m \rangle$ in a small frequency-resolved window $\omega \lesssim 0.05$ and a finite temperature $T = \beta^{-1} = 5J$ ($k_B := 1$). The temperature

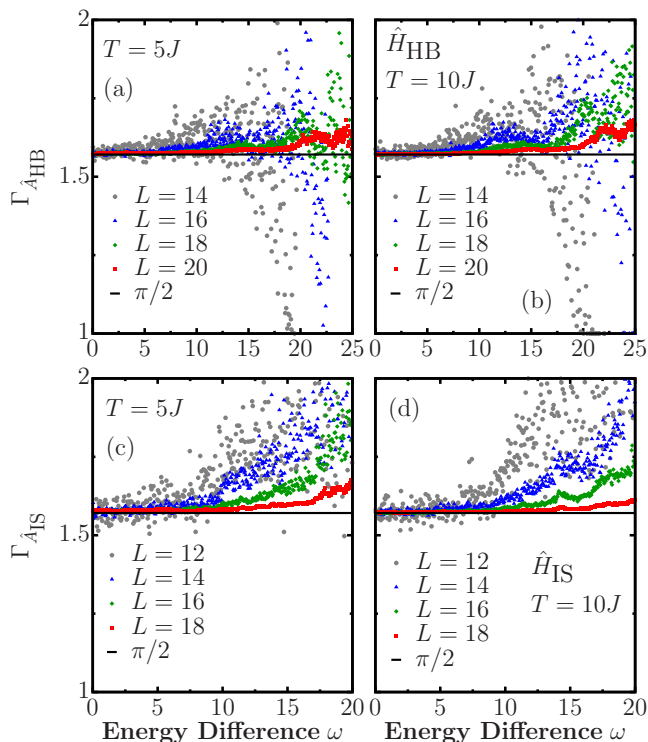


FIG. 2. $\Gamma_{\hat{O}}(\omega)$, from Eq. (6), for local operators \hat{A}_{HB} [(a) and (b)] and \hat{A}_{IS} [(c) and (d)] in the eigenbasis of \hat{H}_{HB} and \hat{H}_{IS} , respectively. Two different finite temperatures were chosen, $T = 5J$ [(a) and (c)] and $T = 10J$ [(b) and (d)]. The matrix elements were computed in a small energy window 0.05ϵ where $\epsilon := E_{\text{max}} - E_{\text{min}}$, and a frequency window $\delta\omega = 0.05$.

is calculated by associating the average energy \bar{E} with a canonical density matrix $\hat{\rho} = e^{-\beta\hat{H}}/Z$ as $\bar{E} = \text{Tr}[\hat{\rho}\hat{H}]$. In Fig. 1 we show the probability distributions obtained by this procedure. We see that the matrix elements are Gaussian-distributed for both local and extensive operators in both of the models we have studied, as has previously been found for other models and observables [32–38]. In order to understand if this property pertains to the entire spectrum away from zero frequency and if the same distributions are observed at all temperatures where the ETH is expected to hold, we proceed to evaluate the frequency-dependent ratio [33]

$$\Gamma_{\hat{O}}(\omega) := \overline{|O_{nm}|^2} / \overline{|O_{nm}|}^2, \quad (6)$$

where the averages are performed over a small frequency window $\delta\omega = 0.05$. Should the individual matrix elements be Gaussian-distributed with zero mean at a given value of ω , then $\Gamma_{\hat{O}}(\omega) = \pi/2$.

In Fig. 2 we show the $\Gamma_{\hat{O}}(\omega)$ ratio as a function of frequency $\omega = E_m - E_n$ and of system size L for both \hat{H}_{HB} [panels (a) and (b)] and \hat{H}_{IS} [panels (c) and (d)], evaluated for the local operators \hat{A}_{HB} and \hat{A}_{IS} from Eq. (4) and for two different temperatures $T = 5J$

and $T = 10J$ (similar results are obtained for \hat{B} operators [42]). Gaussian statistics emerge at all frequencies, i.e. $\Gamma_{\hat{O}} \approx \pi/2$ for increasing values of ω as the system size increases. These findings, together with recent results that have highlighted normality in the distributions of off-diagonal matrix elements in the high-temperature limit [33, 35, 36, 38], strongly suggest that Gaussianity is ubiquitous in non-integrable models for which the ETH is expected to hold, even at finite temperature.

Matrix-element correlations.—Let us now examine the overall structure of the statistical matrix R_{nm} as a function of the mean energy $\bar{E} = (E_m + E_n)/2$ and transition frequency $\omega = E_m - E_n$. In particular, we are interested in correlations between matrix elements at different frequencies, which are encoded in the eigenvalue distribution of the matrix O_{nm} . In the absence of correlations, the eigenvalue distribution should coincide with that of the Gaussian orthogonal ensemble (GOE), where each matrix element is an independent, identically distributed random variable [46]. Therefore, any deviation from the GOE prediction heralds the presence of correlations between matrix elements.

In order to investigate the temperature- and frequency-dependence of such correlations, we consider submatrices of \hat{O} restricted to a finite frequency window and construct the corresponding eigenvalue distributions, following Ref. [29]. To fix the temperature, we first extract a $\mathcal{D}' \times \mathcal{D}'$ submatrix from \hat{O} , centred around the diagonal matrix element O_{nn} such that $E_n = \text{Tr}[\hat{\rho}\hat{H}]$. The size \mathcal{D}' of this submatrix is selected to encompass an energy range of width 0.125ϵ , where $\epsilon := E_{\text{max}} - E_{\text{min}}$ is the bandwidth. We then further restrict our attention to frequencies $|\omega| < \omega_c$ by setting

$$O_{nm}^{\omega_c} := \begin{cases} O_{nm}, & \text{if } |E_m - E_n| < \omega_c \\ 0, & \text{otherwise.} \end{cases} \quad (7)$$

To test for correlations between these matrix elements, we follow the procedure introduced in Ref. [29]: we generate a sign-randomised matrix

$$\tilde{O}_{nm}^{\omega_c} := \begin{cases} O_{nm}^{\omega_c}, & \text{probability} = 1/2, \\ -O_{nm}^{\omega_c}, & \text{probability} = 1/2. \end{cases} \quad (8)$$

The random sign destroys correlations between matrix elements, leading to the semi-elliptical eigenvalue distribution that is characteristic of the GOE [46, 47]. Comparing the eigenvalue distributions of $O_{nm}^{\omega_c}$ and $\tilde{O}_{nm}^{\omega_c}$ thus probes correlations between the matrix elements of \hat{O} within a frequency range controlled by the cutoff ω_c .

The eigenvalues $\{\lambda\}$ of the submatrices (7) and (8) are evaluated numerically and the corresponding distributions, $P_{\omega_c}(\lambda)$, are plotted in Fig. 3 for extensive operators (similar results for local operators are presented in [42]). The eigenvalues of the entire submatrix within the chosen energy window show a clear departure from the semi-elliptical distribution (Fig. 3[(a),(b)] for \hat{B}_{HB}

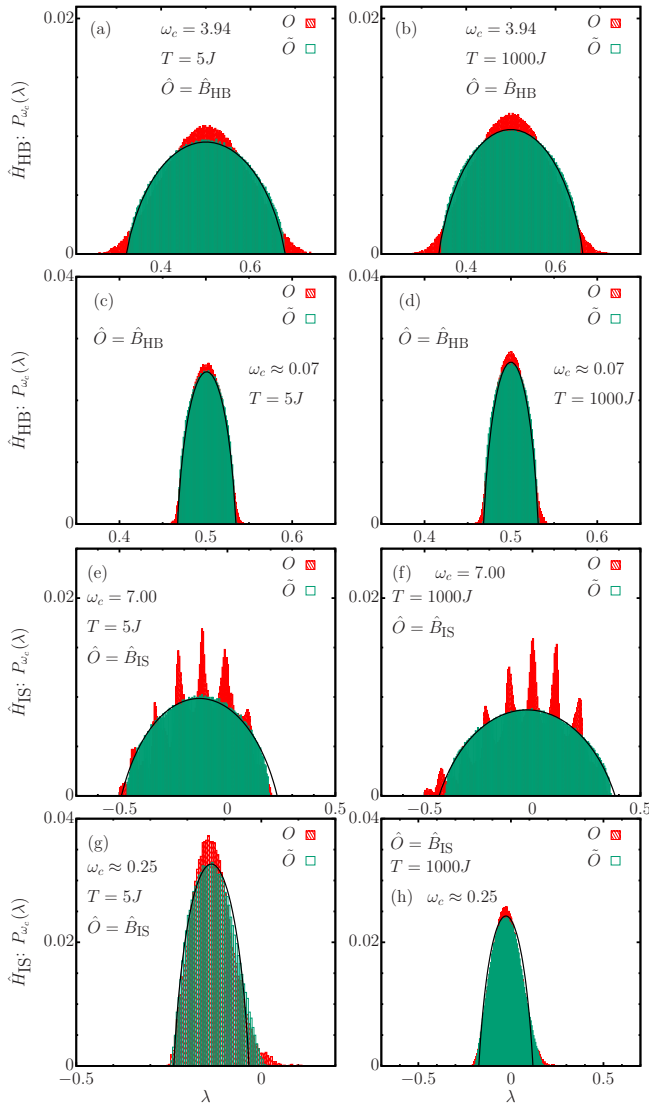


FIG. 3. Probability distributions $P_{\omega_c}(\lambda)$ of the eigenvalues of the full and randomised submatrices [Eqs. (7) and (8)] in an energy window 0.125ϵ for \hat{B}_{HB} [(a), (b)] and \hat{B}_{IS} [(e), (f)]. In [(c), (d)] and [(g), (h)] we show $P_{\omega_c}(\lambda)$ for the banded operators \hat{B}_{HB} and \hat{B}_{IS} , respectively, with the smallest cutoff frequency ω_c such that the eigenvalue distribution follows the GOE (see [42]). All the panels on the left correspond to $T = 5$, while $T = 1000$ for the panels on the right. We show the results for $L = 18$ in \hat{H}_{HB} and $L = 16$ in \hat{H}_{IS} .

and Fig. 3[(e),(f)] for \hat{B}_{IS}), signalling substantial correlations between matrix elements at significantly different frequencies. These correlations are seen for high ($T = 1000J$) and low ($T = 5J$) temperatures alike. For smaller values of the cutoff ω_c , however, the eigenvalue distributions begin to resemble the GOE prediction (Fig. 3[(c),(d)] for \hat{B}_{HB} and Fig. 3[(g),(h)] for \hat{B}_{IS}). Our data are therefore consistent with a crossover to Gaussian random-matrix-like behaviour at low frequencies [29]. The frequency scale of the crossover can be estimated

from the value of ω_c at which the distributions appear to coincide with the GOE prediction, $\omega_c = \omega_{GOE}$. Note that, for even smaller values of ω_c , the eigenvalue statistics eventually become Poissonian due to well-known localisation effects [7] (see [42] for details).

OTOC dynamics.—We now study the implications of these results for the observable dynamics. As discussed above, two-point correlation functions are completely independent of the statistical correlations between matrix elements. It is thus crucial to examine higher-order correlators and the OTOC is a natural example. We focus in particular on the squared commutator

$$c(t) := - \left(\langle [\hat{O}(t), \hat{O}]^2 \rangle - \langle [\hat{O}(t), \hat{O}] \rangle^2 \right). \quad (9)$$

In order to detect the dynamical effect of matrix-element correlations we compute $c(t)$ in two different ways: *i*) by a thermal average in the canonical ensemble at temperature T , and *ii*) using a single eigenstate $|E_n\rangle$ and assuming independent, identically distributed Gaussian statistics for R_{nm} in the ETH Eq. (1) [26, 27, 48], which leads to an expression for the OTOC in terms of two-point functions (see Ref. [42] for details). The result of this comparison is shown in Fig. 4 for sums of local operators. A clear discrepancy between the two predictions at

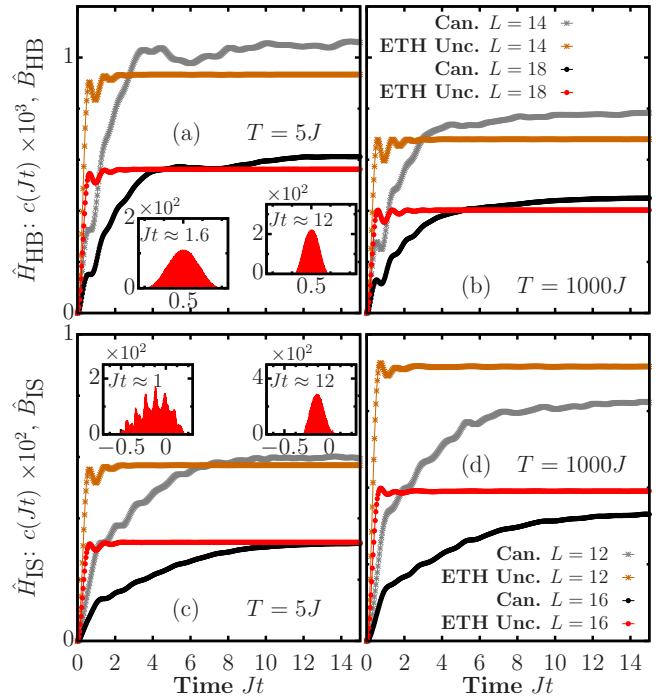


FIG. 4. Time-dependent square-commutator (9) for the operators \hat{B}_{HB} [(a),(b)] and \hat{B}_{IS} [(c),(d)] for \hat{H}_{HB} and \hat{H}_{IS} at temperatures $T = 5J$ [(a) and (c)] and $T = 1000J$ [(b) and (d)]. The expectation value obtained for a canonical state is compared with the one obtained assuming the ETH and uncorrelated R_{nm} for increasing system size L . Insets show the distribution of eigenvalues of the matrix $\hat{O}^{\omega_c = 2\pi/t}$ (7) for the largest system size displayed in each case.

short times signals that this regime is indeed governed by correlations between the matrix elements. However, the curves saturate to a similar value at longer times, differing in some cases by a small correction that we attribute to energy fluctuations in the canonical ensemble at finite size [42]. Fig. 4 shows that the time t_s at which saturation occurs qualitatively increases with system size.

Interestingly, our data suggest that this saturation time is related to the frequency ω_{GOE} by $t_s \approx 2\pi/\omega_{\text{GOE}}$. Since the limited availability of system sizes does not allow to study systematically the relation and scaling of t_s and ω_{GOE} (though they are roughly numerically consistent), we proceed visually by showing the distribution of eigenvalues of the matrix $\hat{O}^{\omega_c=2\pi/t}$ at different times (insets of Fig. 4). While at short times the distribution deviates from the GOE prediction, these deviations are strongly reduced when the OTOC nears saturation. This behaviour indicates that the OTOC's long-time dynamics encodes the statistical properties of R_{nm} and the emergence of random-matrix behaviour at low frequencies.

Conclusions.— In this letter, we have performed a systematic analysis of statistical correlations within the ETH in realistic models of thermalising systems, and explored their consequences for the dynamics of quantum

information scrambling. Remarkably, we find that correlations between off-diagonal matrix elements indicate the timescale for the onset of random-matrix dynamics in the corresponding OTOC, an experimentally observable quantity. This operator-dependent timescale is not apparently connected to hydrodynamic behaviour of linear-response functions and, although a precise finite-size scaling is currently lacking, our results suggest that it reflects the growth of operator complexity beyond the Thouless time [49].

Acknowledgements.—M. B. and J. G. acknowledge the Department of Jobs, Enterprise and Innovation/Department of Education and Skills/Science Foundation of Ireland/Higher Education Authority (DJEI/DES/SFI/HEA) Irish Centre for High-End Computing (ICHEC) for the provision of computational facilities and support, Project No. TCPHY118B, and the Trinity Centre for High-Performance Computing. This work was supported by a SFI-Royal Society University Research Fellowship (J. G.) and the Royal Society (M. B.). J. G. acknowledges funding from European Research Council Starting Grant ODYSSEY (Grant Agreement No. 758403).

* brenesnm@tcd.ie

† silvia.pappalardi@phys.ens.fr

- [1] E. Schrödinger, *Annalen der Physik* **388**, 956 (1927).
- [2] J. v. Neumann, *Zeitschrift für Physik* **57**, 30 (1929).
- [3] M. Rigol, V. Dunjko, and M. Olshanii, *Nature* **452**, 854 (2008).
- [4] A. Polkovnikov, K. Sengupta, A. Silva, and M. Vengalattore, *Reviews of Modern Physics* **83**, 863 (2011).
- [5] J. Eisert, M. Friesdorf, and C. Gogolin, *Nature Physics* **11**, 124 (2015).
- [6] F. Borgonovi, F. Izrailev, L. Santos, and V. Zelevinsky, *Physics Reports* **626**, 1 (2016).
- [7] L. D'Alessio, Y. Kafri, A. Polkovnikov, and M. Rigol, *Advances in Physics* **65**, 239 (2016).
- [8] T. Kinoshita, T. Wenger, and D. S. Weiss, *Nature* **440**, 900 (2006).
- [9] M. Lewenstein, A. Sanpera, V. Ahufinger, B. Damski, A. Sen, and U. Sen, *Advances in Physics* **56**, 243 (2007).
- [10] I. Bloch, J. Dalibard, and S. Nascimbene, *Nature Physics* **8**, 267 (2012).
- [11] J. L. Lebowitz and O. Penrose, *Physics Today* **26**, 23 (1973).
- [12] J. M. Deutsch, *Physical Review A* **43**, 2046 (1991).
- [13] M. Srednicki, *Physical Review E* **50**, 888 (1994).
- [14] M. Srednicki, *Journal of Physics A: Mathematical and General* **32**, 1163 (1999).
- [15] B. Swingle, *Nature Physics* **14**, 988 (2018).
- [16] P. Hosur, X.-L. Qi, D. A. Roberts, and B. Yoshida, *Journal of High Energy Physics* **2016** (2016).
- [17] D. E. Parker, X. Cao, A. Avdoshkin, T. Scaffidi, and E. Altman, *Phys. Rev. X* **9**, 041017 (2019).
- [18] A. Larkin and Y. N. Ovchinnikov, *Soviet Physics JETP* **28**, 1200 (1969).
- [19] A. Kitaev, "Hidden Correlations in the Hawking Radiation and Thermal Noise (2:00)," <https://www.youtube.com/watch?v=0Q9qN8j7EZI> (2015).
- [20] S. H. Shenker and D. Stanford, *Journal of High Energy Physics* **2014**, 67 (2014).
- [21] J. Maldacena, S. H. Shenker, and D. Stanford, *Journal of High Energy Physics* **2016**, 106 (2016).
- [22] M. Gärttner, J. G. Bohnet, A. Safavi-Naini, M. L. Wall, J. J. Bollinger, and A. M. Rey, *Nature Physics* **13**, 781 (2017).
- [23] J. Li, R. Fan, H. Wang, B. Ye, B. Zeng, H. Zhai, X. Peng, and J. Du, *Physical Review X* **7**, 031011 (2017).
- [24] X. Nie, B.-B. Wei, X. Chen, Z. Zhang, X. Zhao, C. Qiu, Y. Tian, Y. Ji, T. Xin, D. Lu, and J. Li, *Physical Review Letters* **124**, 250601 (2020).
- [25] X. Mi, P. Roushan, C. Quintana, S. Mandra, J. Marshall, C. Neill, F. Arute, K. Arya, J. Atalaya, R. Babbush, *et al.*, *arXiv preprint arXiv:2101.08870* (2021).
- [26] L. Foini and J. Kurchan, *Physical Review E* **99**, 042139 (2019).
- [27] C. Murthy and M. Srednicki, *Physical Review Letters* **123**, 230606 (2019).
- [28] A. Chan, A. De Luca, and J. T. Chalker, *Physical Review Letters* **122**, 220601 (2019).
- [29] J. Richter, A. Dymarsky, R. Steinigeweg, and J. Gemmer, *Physical Review E* **102**, 042127 (2020).
- [30] E. Khatami, G. Pupillo, M. Srednicki, and M. Rigol, *Physical Review Letters* **111**, 050403 (2013).
- [31] H. Kim and D. A. Huse, *Physical Review Letters* **111**, 127205 (2013).
- [32] W. Beugeling, R. Moessner, and M. Haque, *Physical Review E* **91**, 012144 (2015).
- [33] T. LeBlond, K. Mallayya, L. Vidmar, and M. Rigol,

- Physical Review E **100**, 062134 (2019).
- [34] I. M. Khaymovich, M. Haque, and P. A. McClarty, *Physical Review Letters* **122**, 070601 (2019).
 - [35] M. Brenes, T. LeBlond, J. Goold, and M. Rigol, *Physical Review Letters* **125**, 070605 (2020).
 - [36] T. LeBlond and M. Rigol, *Physical Review E* **102**, 062113 (2020).
 - [37] L. F. Santos, F. Pérez-Bernal, and E. J. Torres-Herrera, *Physical Review Research* **2**, 043034 (2020).
 - [38] M. Brenes, J. Goold, and M. Rigol, *Physical Review B* **102**, 075127 (2020).
 - [39] D. J. Luitz and Y. Bar Lev, *Physical Review Letters* **117**, 170404 (2016).
 - [40] D. J. Luitz, *Physical Review B* **93** (2016).
 - [41] L. Foini and J. Kurchan, *Physical Review Letters* **123** (2019).
 - [42] See the Supplemental Material at [] for additional information about diagonal matrix elements of local and collective observables in the energy eigenbasis, real time dynamics of two-point functions and finite-size corrections, Gaussianity indicators for operators composed of local operators, localisation effects for eigenvalue distributions of \hat{O}^{ω_c} , further results for frequency-resolved eigenvalue distributions for local observables and details on the computation of the square commutator with the assumption of uncorrelated statistics, backed with further numerical evaluation for the case of local observables. The Supplemental Material contains Refs. [7, 14, 27, 29, 30, 33, 35, 38, 43, 45, 50, 51].
 - [43] R. Mondaini and M. Rigol, *Physical Review E* **96**, 012157 (2017).
 - [44] T. LeBlond and M. Rigol, *Physical Review E* **102**, 062113 (2020).
 - [45] M. Brenes, S. Pappalardi, J. Goold, and A. Silva, *Physical Review Letters* **124**, 040605 (2020).
 - [46] M. L. Mehta, *Random matrices* (Elsevier, 2004).
 - [47] G. Livan, M. Novaes, and P. Vivo, *Introduction to Random Matrices* (Springer International Publishing, 2018).
 - [48] J. Cotler, N. Hunter-Jones, J. Liu, and B. Yoshida, *Journal of High Energy Physics* **2017** (2017).
 - [49] A. Dymarsky, [arXiv:1804.08626](https://arxiv.org/abs/1804.08626) [cond-mat.stat-mech] (2018).
 - [50] C. Schönle, D. Jansen, F. Heidrich-Meisner, and L. Vidmar, [arXiv preprint arXiv:2011.13958](https://arxiv.org/abs/2011.13958) (2020).
 - [51] S. Pappalardi, A. Polkovnikov, and A. Silva, *SciPost Physics* **9** (2020).

Supplemental Material: Out-of-time-order correlations and the fine structure of eigenstate thermalisation

Marlon Brenes¹, Silvia Pappalardi², Mark T. Mitchison¹, John Goold¹ and Alessandro Silva³

¹*Department of Physics, Trinity College Dublin, Dublin 2, Ireland*

²*Laboratoire de Physique de l'École Normale Supérieure, Paris, France*

³*SISSA, Via Bonomea 265, I-34135 Trieste, Italy*

In this Supplemental Material, we provide additional information on the numerical computations and on the analytical estimates discussed in the main text, based on the ETH [7, 14]:

$$O_{nm} = O(\bar{E})\delta_{nm} + e^{-S(\bar{E})/2} f_{\hat{O}}(\bar{E}, \omega) R_{nm}, \quad (\text{S1})$$

where both $O(\bar{E})$ and $f_{\hat{O}}(\bar{E}, \omega)$ are smooth functions of their arguments $\bar{E} = (E_n + E_m)/2$ and $\omega = E_m - E_n$, $S(\bar{E})$ is the microcanonical entropy, and R_{nm} is a pseudo-random statistical matrix with zero average and unit variance.

In Sec. S1, we study the diagonal matrix elements of local and collective observables in the energy eigenbasis, showing that the two models under analysis obey ETH. In Sec. S2, we consider the real-time dynamics of two point functions and we compare the exact calculation for a thermal state with the result predicted by ETH. Finite-size corrections are evaluated in Sec. S3. In Sec. S4, we report the results for $\Gamma_{\hat{O}}(\omega)$ for operators made of sums of local operators. In Sec. S5 we study the localisation effects on the eigenvalues distribution of \hat{O}^{ω_c} below a given frequency threshold. In Sec. S6, we discuss other details for the computation of the statistics of the matrix elements. In Sec. S7, we report further results regarding the correlations of the matrix elements in the case of local operators. We conclude with Sec. S8 with the expression of the square-commutator with the assumption of uncorrelated statistics and further details on the numerical computation of four-point functions.

S1. DIAGONAL MATRIX ELEMENTS OF OBSERVABLES

A strong indication of eigenstate thermalisation is the behaviour of diagonal matrix elements of observables in the eigenbasis of the Hamiltonian [7, 33, 35]. In Fig. S1 we show the diagonal matrix elements of \hat{A}_{HB} [panel (a)] and of \hat{A}_{IS} [panel (b)] for the non-integrable models studied in this work [Eqs. (2) and (3) in the main text]. We defined the energy density $\epsilon_n := (E_n - E_{\text{min}})/(E_{\text{max}} - E_{\text{min}})$ and computed all the matrix elements in the eigenbasis of the Hamiltonian by full diagonalisation. It can be observed that, as the system size L is increased, the support over which the matrix elements exist shrink. This observation strongly suggests that in the thermodynamic limit, the diagonal matrix elements can be described by a

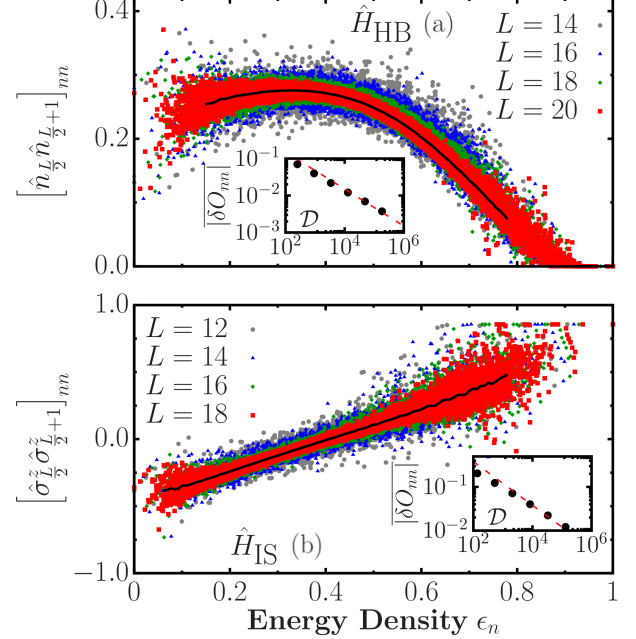


FIG. S1. Diagonal matrix elements of \hat{A}_{HB} (a) and \hat{A}_{IS} (b) as a function of the energy density $\epsilon_n := (E_n - E_{\text{min}})/(E_{\text{max}} - E_{\text{min}})$ and of the system size L . The black lines depict an approximation of the smooth function $O(\bar{E})$ obtained from a coarse-grained average of the data for the largest system size. The insets show the eigenstate-to-eigenstate fluctuations for different systems sizes, obtained from the eigenvalues in the central region. The dashed lines on the insets show the $\mathcal{D}^{-1/2}$ scaling.

smooth function $O(\bar{E})$ corresponding to the microcanonical prediction (note that the second term in Eq. (1) is exponentially suppressed in Hilbert space dimension \mathcal{D}). The black lines in Fig. S2 depict an approximation of the smooth function $O(\bar{E})$, obtained from a coarse-grained average of the data for the largest system size.

The insets in Fig. S1 highlight the trend of the absolute value of the eigenstate-to-eigenstate fluctuations, defined as

$$|\delta O_{nn}| := |O_{nn} - O_{n+1n+1}|, \quad (\text{S2})$$

computed for 20% of the total eigenvalues in the centre of the spectrum. The dashed line on the insets in Fig. S1 corresponds to the scaling $\mathcal{D}^{-1/2}$, expected in the high-temperature regime of non-integrable models.

The corresponding results for sums of local operators,

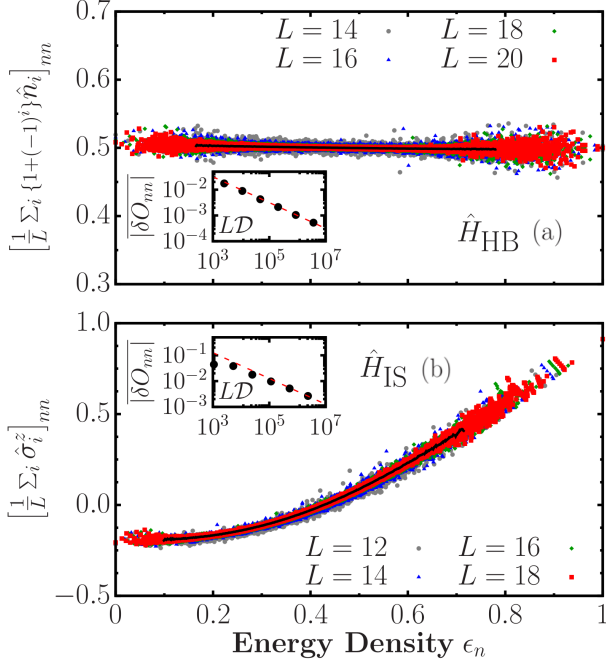


FIG. S2. Diagonal matrix elements of \hat{B}_{HB} (a) and \hat{B}_{IS} (b) as a function of the energy density $\epsilon_n := (E_n - E_{\text{min}})/(E_{\text{max}} - E_{\text{min}})$ and of the system size L . The black lines depict an approximation of the smooth function $O(E)$ obtained from a coarse-grained average of the data for the largest system size. The insets show the eigenstate-to-eigenstate fluctuations for different systems sizes, obtained from the eigenvalues in the central region. The dashed lines on the insets show the $(LD)^{-1/2}$ scaling.

\hat{B}_{HB} [panel (a)] and \hat{B}_{IS} [panel (b)] are shown in Fig. S2. Analogous results as described before are observed, with the exception that the support over which the diagonal matrix elements exist is much smaller than for local observables. A difference to be highlighted concerns the insets in Fig. S2. The eigenstate-to-eigenstate fluctuations for these class of observables in the high-temperature regime is expected to scale as $(LD)^{-1/2}$, due to the $1/\sqrt{L}$ scaling of the Schmidt norm [33, 35]. The insets in Fig. S2 contain a dashed line that depicts the $(LD)^{-1/2}$ scaling of $|\overline{\delta O_{nm}}|$, and, as can be observed, such trend is followed the numerical data.

The results shown in Figs. S1 and S2 indicate that the ETH is obeyed by the models and observables considered in the main text for the parameters selected, away from non-generic features observed at the edges of the spectrum.

S2. DYNAMICS OF TWO-POINT CORRELATION FUNCTIONS

The ETH in Eq. (1) provides the form of the off-diagonal matrix elements required to predict the dynamics of two-point correlation functions at thermal equilib-

rium. We are interested in correlation functions of the form

$$F_2(t) := \langle \hat{O}(t) \hat{O}(0) \rangle_c := \langle \hat{O}(t) \hat{O}(0) \rangle - \langle \hat{O}(t) \rangle \langle \hat{O}(0) \rangle, \quad (\text{S3})$$

where the expectation values are evaluated in one of the ensembles of statistical mechanics. One could, for instance, consider the canonical ensemble. For an operator \hat{A} in such case, we have that $\langle \hat{A} \rangle = \text{Tr}[\hat{\rho} \hat{A}]$, where $\hat{\rho} = e^{-\beta \hat{H}}/Z$ is the density matrix operator for a system with Hamiltonian \hat{H} , partition function $Z = \text{Tr}[e^{-\beta \hat{H}}]$ and inverse temperature $\beta = 1/T$. In Eq. (S3), the operators are written in the Heisenberg picture $\hat{O}(t) = e^{i\hat{H}t} \hat{O}(0) e^{-i\hat{H}t}$.

On the other hand, eigenstate thermalisation suggests that such expectation values could be evaluated for a *single eigenstate* $|E_n\rangle$. The evaluation is simpler if one instead considers the symmetric and anti-symmetric response functions which yield, respectively, the real and imaginary parts of $F_2(t)$. Written in such fashion we have

$$\begin{aligned} S_{\hat{O}}^+(E_n, t) &:= \langle E_n | \{ \hat{O}(t), \hat{O}(0) \} | E_n \rangle_c = 2 \text{Re}[F_2(E_n, t)] \\ S_{\hat{O}}^-(E_n, t) &:= \langle E_n | [\hat{O}(t), \hat{O}(0)] | E_n \rangle_c = 2i \text{Im}[F_2(E_n, t)], \end{aligned} \quad (\text{S4})$$

where $\{\cdot, \cdot\}$ and $[\cdot, \cdot]$ stand for the anti-commutator and commutator, respectively. In this notation, $F_2(t)$ is the one considered in the canonical ensemble, while $F_2(E_n, t)$ is the one evaluated for a single energy eigenstate.

Following the standard derivation [7, 14, 50] from the ETH in Eq. (1), one obtains the correlation functions in frequency domain in the thermodynamic limit

$$\begin{aligned} S_{\hat{O}}^+(E_n, \omega) &\approx 4\pi \cosh(\beta\omega/2) |f_{\hat{O}}(E_n, \omega)|^2, \\ S_{\hat{O}}^-(E_n, \omega) &\approx 4\pi \sinh(\beta\omega/2) |f_{\hat{O}}(E_n, \omega)|^2. \end{aligned} \quad (\text{S5})$$

Given that these relations are symmetric and anti-symmetric, respectively, their Fourier transforms to yield the correlation functions in the time domain are simplified to

$$\begin{aligned} \text{Re}[F_2(E_n, t)] &= \int_0^\infty d\omega \cos(\omega t) S_{\hat{O}}^+(E_n, \omega), \\ \text{Im}[F_2(E_n, t)] &= \int_0^\infty d\omega \sin(\omega t) S_{\hat{O}}^-(E_n, \omega). \end{aligned} \quad (\text{S6})$$

At this point is important to make two observations with respect to Eq. (S6). First, in the thermodynamic limit we expect $F_2(E_n, t) = F_2(t)$. This immediately follows from the association of the energy E_n to a corresponding canonical inverse temperature β by assigning $E_n = \langle E \rangle = \text{Tr}[\hat{H} e^{-\beta \hat{H}}]/Z$. Second, in Eq. (S5), there is no dependency of the random variable R_{nm} . This follows from the fact that this term enters the dynamical correlations in the form of the average of $|R_{nm}|^2$, which is unity by assumption [7, 14]. Indeed, it suffices that

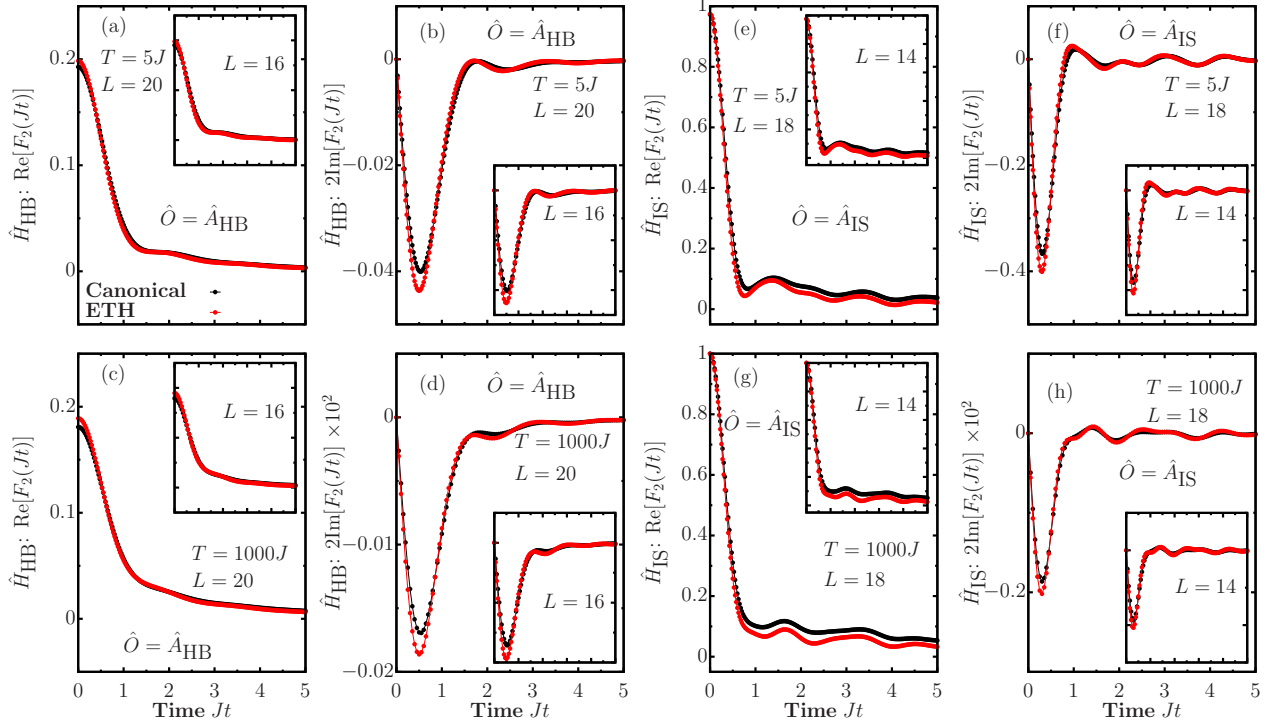


FIG. S3. Dynamics of the two-point correlation function evaluated in the canonical ensemble at temperature T and in the ETH with a compatible energy density for local operators. In [(a)-(d)] we show the results for \hat{H}_{HB} and in [(e)-(h)] the corresponding results for \hat{H}_{IS} at different temperatures for different system sizes as highlighted in the figure.

this random variable has a well-defined variance for the $|R_{nm}|^2$ term to vanish from the final expressions.

The equivalency between the dynamics of two-point correlation functions in statistical mechanics and the corresponding dynamics of the same object predicted by the ETH can be observed in generic systems. Following Eqs. (S5) and (S6), the dynamics of the correlation functions depend solely on the function of $f_{\hat{O}}(E_n, \omega)$; which is, in general, system- and observable-dependent. A commonly-used procedure [30, 35, 38, 43, 45] to isolate this function in generic systems involves a frequency-resolved analysis of the matrix elements of a given observable in the energy eigenbasis. One focuses on a small window of energies and extracts the off-diagonal matrix elements of an operator \hat{O} in the eigenbasis of the Hamiltonian. For finite-size systems, the fluctuations present are accounted for by considering not a single eigenstate, but a collection of eigenstates around a given energy E_n . A coarse-grained average then leads to a smooth function $e^{-S(E_n)/2} f_{\hat{O}}(E_n, \omega)$. The entropy term, $e^{-S(E_n)/2}$, is not a function of ω and in principle needs to be evaluated. Instead of evaluating this term directly, we first compute the symmetric correlation function $S_{\hat{O}}^+(E_n, \omega)$ and normalise it by the sum rule

$$\int_{-\infty}^{\infty} d\omega S_{\hat{O}}^+(E_n, \omega) = 4\pi \left[\langle E_n | \hat{O}^2 | E_n \rangle - \langle E_n | \hat{O} | E_n \rangle^2 \right], \quad (\text{S7})$$

while the anti-symmetric correlation function $S_{\hat{O}}^-(E_n, \omega)$ follows from Eq. (S5), which is the manifestation of the fluctuation-dissipation theorem.

This procedure can be applied to the models and observables described in the main text. In Fig. S3, we show the dynamics of both the real and imaginary parts of the two-time correlation function in Eq. (S3), for the local observables in Eq. (4) of the main text. The dynamics of the two-point correlation function in the canonical ensemble were evaluated by direct diagonalisation of the propagator $e^{-i\hat{H}t}$ acting on the density operator $\hat{\rho}$, while the dynamics from the ETH were evaluated using the procedure described above. For the latter, we computed $e^{-S(E_n)/2} f_{\hat{O}}(E_n, \omega)$ by considering a target energy $\bar{E} = \text{Tr}[\hat{\rho}\hat{H}]$ consistent with the canonical temperature T and averaging all the off-diagonal matrix elements within an energy window of width 0.075ϵ , where $\epsilon := E_{\text{max}} - E_{\text{min}}$ [see Refs. [30, 35, 43, 45] for further details on the extraction of $f_{\hat{O}}(E_n, \omega)$].

For finite-size systems, the connected symmetric correlation function contains a time-independent term that is not present if one evaluates the same object on a single eigenstate. This term is expected to vanish in the thermodynamic limit, see Sec. S3 for an extended discussion.

Though the fine details and the actual form of the decay of $F_2(t)$ depend on the system being considered, it can be observed from Fig. S3 that $F_2(E_n, t) \approx F_2(t)$, an approximation that becomes more accurate as the ther-

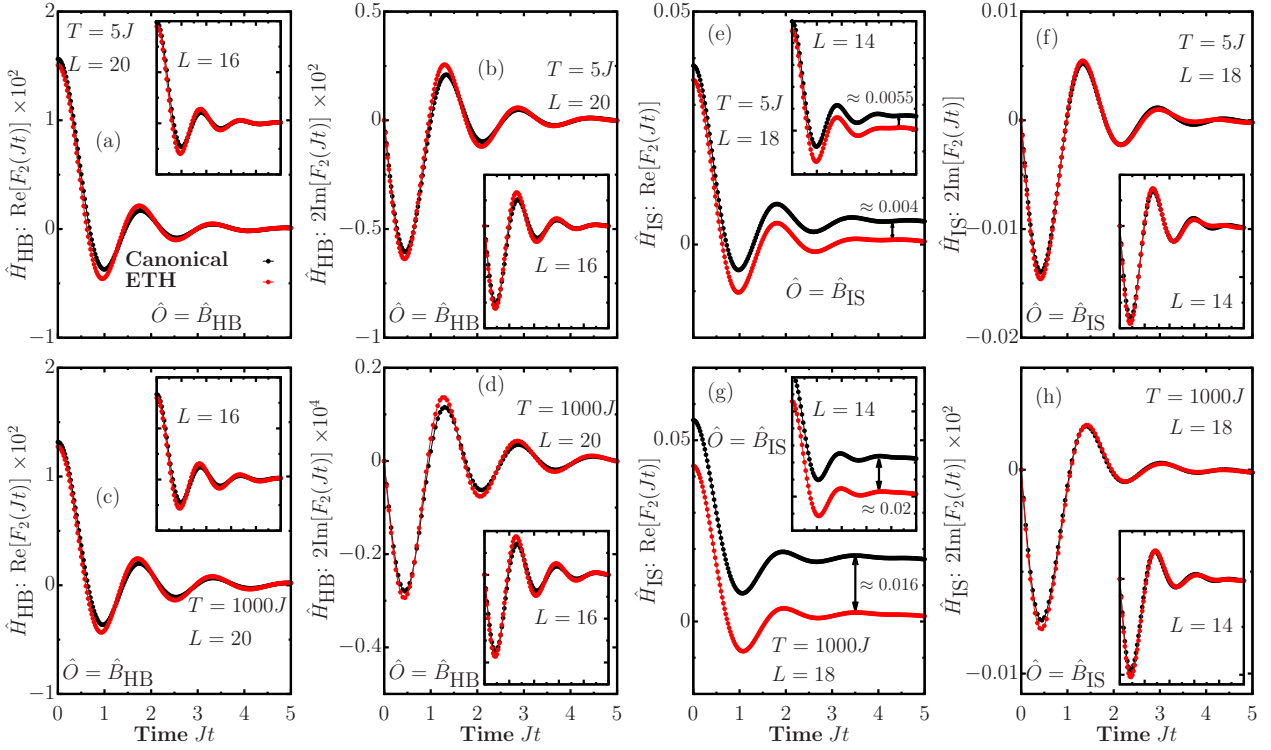


FIG. S4. Dynamics of the two-point correlation function evaluated in the canonical ensemble at temperature T and in the ETH with a compatible energy density for local operators. In [(a)-(d)] we show the results for \hat{H}_{HB} and in [(e)-(h)] the corresponding results for \hat{H}_{IS} at different temperatures for different system sizes as highlighted in the figure.

modynamic limit is approached. It is important to remark that such prediction is accurate not only at high temperature (bottom panels in Fig. S3), but at finite temperature (top panels in Fig. S3) as well.

The ETH can also be applied to study dynamical correlations of two-point functions for observables that are composed of sums of local operators, such as the ones in Eq. (4) of the main text. In Fig. S4 we show the results for the dynamics of two-point functions for this class of observables. As observed before in Fig. S3, the ETH prediction resolves the same features observed when computing the dynamics in the canonical ensemble at finite and high temperatures. A key difference to be highlighted between Fig. S4[(a),(c)] and Fig. S4[(e),(g)] is that, for the latter, there exists a seemingly constant term differing from the results in the canonical ensemble and the ETH prediction. The difference stems from the fluctuations in the canonical ensemble (see Sec. S3), a term which is already small for \hat{B}_{HB} in Fig. S4[(a),(c)], but not as much for \hat{B}_{IS} in Fig. S4[(e),(g)]. The difference, however, as highlighted in Fig. S4[(e),(g)], becomes smaller as the system size is increased. The dynamics observed strongly suggest that such seemingly-constant discrepancy can be attributed to finite-size corrections.

S3. FINITE-SIZE TERM IN SYMMETRIC CORRELATION FUNCTIONS

The symmetric correlation function evaluated on a thermal state $F_2(t)$ [cf. Eq.(S3)] differs from the one computed on a single eigenstate $F_2(E_n, t)$ by a sub-leading term in the thermodynamic limit [7].

The expectation value computed in the canonical ensemble is defined as $\langle \cdot \rangle := \text{Tr}[\hat{\rho} \cdot] = \sum_n p_n \langle E_n | \cdot | E_n \rangle$, where in the case of a canonical density matrix one has $p_n = e^{-\beta E_n} / Z$. In general, other ensembles can be considered, provided that the distribution of the p_n is sufficiently peaked around some average energy $E = \langle \hat{H} \rangle$ with small variance $\delta E^2 = \langle \hat{H}^2 \rangle - \langle \hat{H} \rangle^2$, i.e. $\delta E^2 / E^2 \sim 1/L$. Defining $O_{nm} = \langle E_n | \hat{O} | E_m \rangle$, the two point function Eq. (S3) reads

$$\begin{aligned}
 F_2(t) &= \sum_{nm} p_n e^{-i(E_m - E_n)t} O_{nm} O_{mn} - \left(\sum_n p_n O_{nn} \right)^2 \\
 &= \sum_{n \neq m} p_n e^{-i(E_m - E_n)t} O_{nm} O_{mn} + \langle O^2 \rangle - \langle O \rangle^2 \\
 &= \sum_n p_n \langle E_n | \hat{O}(t) \hat{O} | E_n \rangle_c + \delta O^2, \quad (\text{S8})
 \end{aligned}$$

where in the second line we have identified $\langle O^2 \rangle = \sum_n p_n [O_{nn}]^2$, $\langle O \rangle = \sum_n p_n O_{nn}$ and defined $\delta O^2 :=$

$\langle O^2 \rangle - \langle O \rangle^2$. The first term in Eq. (S8) coincides with the two-point function evaluated on a single eigenstate $F_2(E_n, t)$, while the second one is a time-independent quantity that can be shown to be subleading, i.e.,

$$F_2(t) \sim F_2(E, t) + \mathcal{O}(1/L) \quad \text{for } L \gg 1.$$

Using the ETH in Eq.(1) and the fact that p_n is peaked around energy E , one can write down a Taylor expansion around E and the diagonal elements $O_{nn} = O(E_n)$ as

$$O(E_n) = O(E) + (E_n - E)O'(E) + \frac{(E_n - E)^2}{2}O''(E) + \dots, \quad (\text{S9})$$

where $O'(E)$ and $O''(E)$ are respectively the first and second derivatives with respect to energy of the micro-canonical smooth function $O(E)$ in Eq. (1). It then follows that, to leading order,

$$\delta O^2 = \left(\frac{\partial O}{\partial E} \right)^2 \delta E^2 + \dots \quad (\text{S10})$$

Because we require $\delta E^2/E^2 \sim 1/L$, then it follows that δO^2 is subleading in the thermodynamic limit. For finite-size systems, however, this term corresponds to the time-independent finite-size correction discussed in the previous section, observed in Figs. S3-S4.

S4. GAUSSIAN DISTRIBUTIONS FOR SUMS OF LOCAL OBSERVABLES

We report results for the Gaussianity estimator $\Gamma_{\hat{O}}(\omega)$ [see Eq. (6) in the main text] in Fig. S5 for the second class of observables we have studied in this work, composed of a sum of local operators. For both generic systems under consideration, \hat{H}_{HB} and \hat{H}_{IS} in Eqs. (2) and (3) of the main text, the off-diagonal matrix elements of observables \hat{B}_{HB} and \hat{B}_{IS} in the eigenbasis of their corresponding Hamiltonian are Gaussian-distributed. The similarity with a Gaussian distribution of the matrix elements appears to increase as the system size is increased, suggesting that in the thermodynamic limit these matrix elements are normally distributed for all values of ω . It can also be concluded that the outliers observed for \hat{B}_{IS} in Fig. 1 of the main text are present due to finite-size effects for this particular observable, given that the similarity with a normal distribution increases as the system size is increased.

S5. INFERRING GOE- AND POISSON-DISTRIBUTED FREQUENCY REGIMES FROM THE MEAN RATIO OF LEVEL SPACINGS

Throughout this work, we considered banded submatrices to determine the degree of correlations within the statistical matrix R_{nm} . From Eq. (7) in the main text,

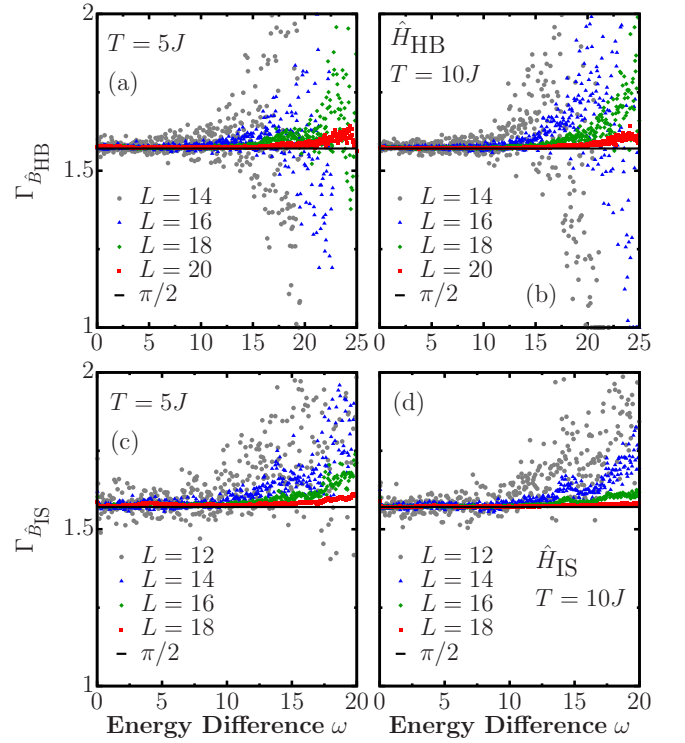


FIG. S5. $\Gamma_{\hat{O}}(\omega)$, from Eq. (6) in the main text, for sums of local operators \hat{B}_{HB} [(a) and (b)] and \hat{B}_{IS} [(c) and (d)] in the eigenbasis of \hat{H}_{HB} and \hat{H}_{IS} , respectively. Two different finite temperatures were chosen, $T = 5J$ [(a) and (c)] and $T = 10J$ [(b) and (d)]. The black horizontal line shows the value $\Gamma_{\hat{O}}(\omega) = \pi/2$. The matrix elements were computed in a small energy window 0.05ϵ where $\epsilon := E_{\text{max}} - E_{\text{min}}$. The binning parameter was selected to be $\delta\omega = 0.05$.

ω_c determines the frequency value associated to a given banded submatrix. We considered ω_c only above a given threshold, due to the fact that below this threshold the eigenvalues of \hat{O}^{ω_c} become uncorrelated because of localisation effects [29]. In this frequency regime, the adjacent eigenvalue level spacings of \hat{O}^{ω_c} are Poisson-distributed.

The relevant frequency regime in the main text is the one dictated by the largest ω_c where the eigenvalues $\lambda_{\alpha}^{\omega_c}$ are still uncorrelated. This implies that there are resonant timescales $t \sim 2\pi/\omega_c$ for which the dynamics are dictated by uncorrelated energy modes. In Ref. [29], it was shown that the eigenvalues of \hat{O}^{ω_c} are uncorrelated even in the regime where the distribution of level spacings follows the GOE. For these reasons, it is important to restrict ourselves to values of ω_c for which the eigenvalues of \hat{O}^{ω_c} are uncorrelated and the level spacings follow the GOE. These regimes can be probed by studying the mean ratio of adjacent level spacings, defined as

$$\langle r_{\omega_c} \rangle := \frac{1}{M} \sum_{\alpha} \frac{\min\{\Delta_{\alpha}, \Delta_{\alpha+1}\}}{\max\{\Delta_{\alpha}, \Delta_{\alpha+1}\}}, \quad (\text{S11})$$

where $\Delta_{\alpha} = |\lambda_{\alpha+1}^{\omega_c} - \lambda_{\alpha}^{\omega_c}|$. We performed the average over all adjacent level spacings, i.e., $M \approx D'$. We have that

$\langle r_{\omega_c} \rangle \approx 0.53$ for a distribution following the GOE and $\langle r_{\omega_c} \rangle \approx 0.39$ for Poisson-distributed random variables.

In Fig. S6 we show the mean ratio of adjacent level spacings for the \hat{H}_{HB} model as a function of ω_c . It can be observed that for both the local observable \hat{A}_{HB} [Fig. S6(a)] and the sum of local observables \hat{B}_{HB} [Fig. S6(b)], the value of ω_c for which the onset of the GOE is observed is rather similar, even for both values of temperature $T = 5$ and $T = 1000$ chosen. We do not expect this behaviour to be generic. On the contrary, the onset of the GOE is typically observed at different values of ω_c for different system sizes L and observables. To avoid the aforementioned localisation effects, we restricted our analyses to the values of ω_c above the ω_c^{min} denoted in Fig. S6. For all $\omega_c > \omega_c^{\text{min}}$, the associated submatrices exhibit a value of $\langle r_{\omega_c} \rangle \approx 0.53$. This, however, does not imply that the matrix elements display correlations or lack thereof. As we have shown in the main text, there exist a regime for which correlations build up as ω_c is increased above ω_c^{min} . In Fig. S7, we show $\langle r_{\omega_c} \rangle$ for the \hat{H}_{IS} model and both local \hat{A}_{IS} [Fig. S7(a)] and sums of local \hat{B}_{IS} [Fig. S7(b)] observables. Similar results are observed, with the only difference noticed at the specific ω_c^{min} values for which the onset of the GOE mean ratio of level spacings is obtained.

S6. FURTHER DETAILS ON STATISTICS

The distribution of all the \mathcal{D}' eigenvalues $\lambda_{\alpha}^{\omega_c}$ of \hat{O}^{ω_c} is expressed as

$$P_{\omega_c}(\lambda) = \frac{1}{\mathcal{D}'} \sum_{\alpha=1}^{\mathcal{D}'} \delta(\lambda - \lambda_{\alpha}^{\omega_c}), \quad (\text{S12})$$

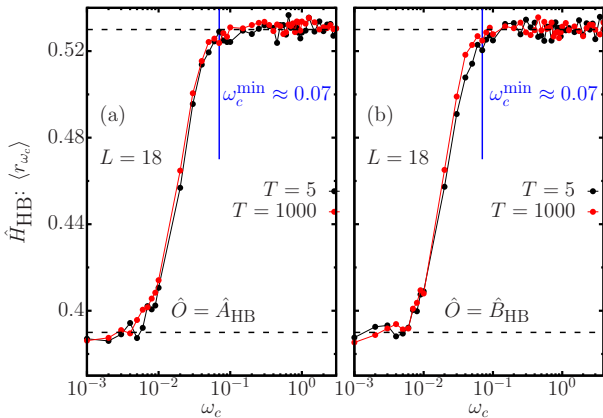


FIG. S6. Mean ratio of adjacent level spacings $\langle r_{\omega_c} \rangle$ as a function of the cutoff frequency ω_c for the \hat{H}_{HB} model, at fixed system size $L = 18$ for two different values of temperature $T = 5$ and $T = 1000$. Panel (a) shows $\langle r_{\omega_c} \rangle$ for the class of local observables \hat{A}_{HB} , while panel (b) shows the results for operator \hat{B}_{HB}

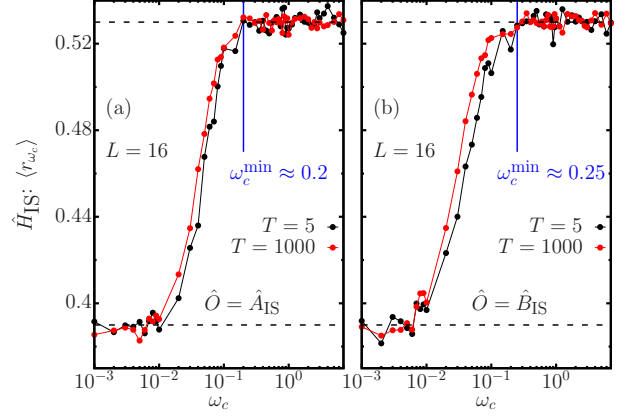


FIG. S7. Mean ratio of adjacent level spacings $\langle r_{\omega_c} \rangle$ as a function of the cutoff frequency ω_c for the \hat{H}_{IS} model, at fixed system size $L = 16$ for two different values of temperature $T = 5$ and $T = 1000$. Panel (a) shows $\langle r_{\omega_c} \rangle$ for the class of local observables \hat{A}_{IS} , while panel (b) shows the results for operator \hat{B}_{IS}

where all the individual $\delta(\cdot)$ peaks are collected in small bins to describe a given probability distribution. The function $P_{\omega_c}(\lambda)$ can be studied as a function of ω_c and yields a semi-circular distribution if the eigenvalues are uncorrelated. If correlations are to arise, deviations from a semi-circle distribution are observed. To compare against a true random matrix, an effective scheme was suggested in Ref. [29]. One proceeds to construct a random matrix from \hat{O}^{ω_c} by assigning a random sign to the matrix elements $O_{nm}^{\omega_c}$ while keeping the operator Hermitian. This defines the operator \tilde{O}^{ω_c} , whose matrix elements are given explicitly by Eq. (8) of the main text.

Even without applying the sign randomisation to the diagonal entries of \hat{O}^{ω_c} , the resulting \tilde{O}^{ω_c} should still resemble a true random matrix; albeit with the added structure of the mean of the distribution of the operator considered. This procedure was not required in Ref. [29] due to the fact that the operator considered had already zero mean in the centre of the spectrum.

S7. CORRELATIONS FOR LOCAL OBSERVABLES

Here, we report the data for the study of matrix correlations for the class of local operators \hat{A}_{HB} and \hat{A}_{IS} in our generic models \hat{H}_{HB} and \hat{H}_{IS} . We show the eigenvalue distributions of \hat{O}^{ω_c} in Fig. S8[(a)-(d)] for \hat{A}_{HB} and in Fig. S8[(e)-(h)] for \hat{A}_{IS} for a single value of $L = 18$ in the case of \hat{H}_{HB} and $L = 16$ for \hat{H}_{IS} . We have selected two values of temperature $T = 5J$ (Fig. S8 panels [(a),(c),(e),(g)]) and $T = 1000J$ (Fig. S8 panels [(b),(d),(f),(h)]). The function $P_{\omega_c}(\lambda)$ is displayed for two different values of ω_c . The larger ω_c value corre-

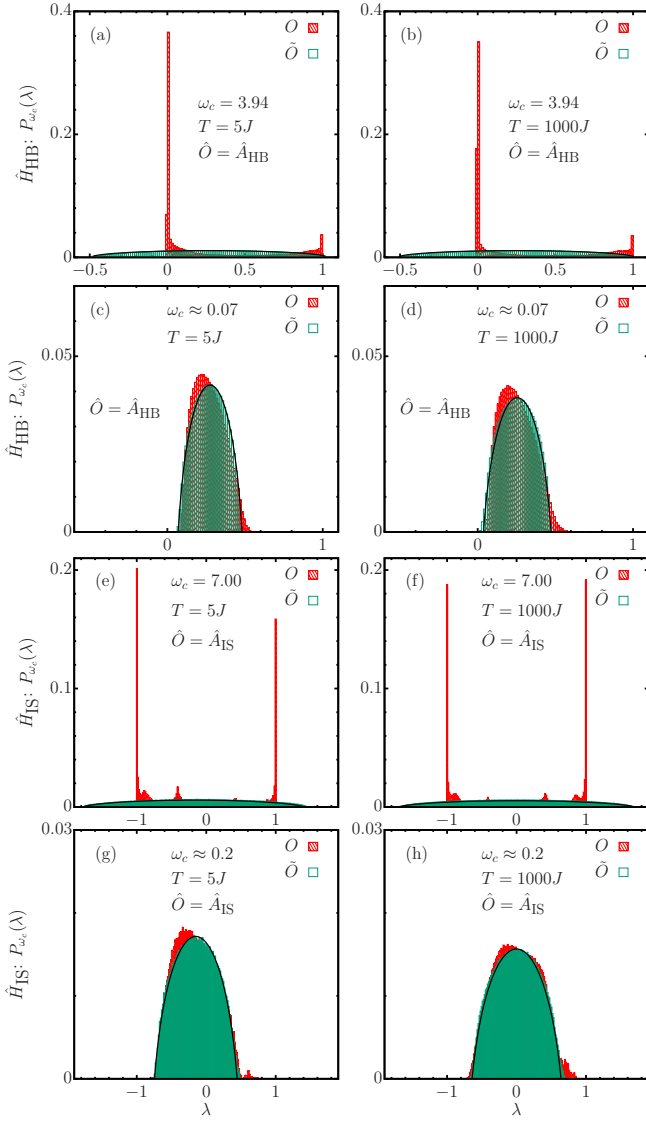


FIG. S8. $P_{\omega_c}(\lambda)$ for the full and randomised submatrices in an energy window 0.125ϵ for \hat{A}_{HB} [(a), (b)] and \hat{A}_{IS} [(e), (f)]. In [(c), (d)] and [(g), (h)] we show $P_{\omega_c}(\lambda)$ for the banded operators \hat{A}_{HB} and \hat{A}_{IS} , respectively, with the smallest cutoff frequency ω_c such that the eigenvalue distribution follows the GOE (see Appendix S5). All the panels on the left correspond to $T = 5J$, while $T = 1000J$ for the panels on the right. We show the results for $L = 18$ in \hat{H}_{HB} and $L = 16$ in \hat{H}_{IS} .

sponds to the frequency value obtained from the entire submatrix in the energy window 0.125ϵ (Fig. S8 panels [(a),(b),(e),(f)]), which differs for different models and observables. The smaller value of ω_c shown (Fig. S8 panels [(c),(d),(g),(h)]), corresponds to the minimum frequency value before localisation effects set in, as shown in Sec. S5.

In Fig. S8 we observe that at larger ω_c values, the eigenvalue distributions expose a high degree of correlations while, at smaller ω_c these correlations disappear. This can be confirmed from the fact that the randomised

operator $\tilde{\hat{O}}^{\omega_c}$ and the true operator \hat{O}^{ω_c} follow a very similar semi-circular distribution (shown as a fitted black line in Fig. S8). This is indeed not the case for larger values of ω_c , for which the distributions are highly peaked at given eigenvalues that depend on the observable and on the temperature. Furthermore, this behaviour persists in the finite- and infinite-temperature regimes. These results suggest that there exists a finite frequency range within which the matrix elements of \hat{O} are effectively uncorrelated.

S8. OUT-OF-TIME-ORDER CORRELATORS

In this section, we evaluate the dynamics of four-point functions to investigate whether correlations translate into an observable effect. We will start by computing the expectation values of time-dependent correlation functions on a single eigenstate, while neglecting any effect of correlations. We will then proceed to evaluate the same objects in the canonical ensemble. The difference in the dynamics will allow us to probe the effect of the correlations exposed in the main text.

A. Four-point functions within Gaussian statistics

In Ref. [27], the ETH result for the thermally-regulated OTOC was computed. It was done by interlacing fractional powers of the density matrix with each operator. The case studied in Ref. [27] had a feature for which the diagonal expectation values vanish, i.e., $O_{nn} = O(E_n) = 0$.

In this work, we considered multi-time correlation functions evaluated on standard thermal states and we generalised the result for cases in which O_{nn} is non-zero. Consider the following four point connected correlator

$$F_c(t_1, t_2, t_3, t_4) \equiv \langle \hat{O}(t_1) \hat{O}(t_2) \hat{O}(t_3) \hat{O}(t_4) \rangle - \langle \hat{O}(t_1) \hat{O}(t_2) \rangle \langle \hat{O}(t_3) \hat{O}(t_4) \rangle \quad (\text{S13})$$

where all operators are written in the Heisenberg representation, $\hat{O}(t) = e^{i\hat{H}t} \hat{O} e^{-i\hat{H}t}$. All time-ordered and out-of-time-ordered correlation functions can be constructed from F_c with a suitable choice of arguments. In particular, we focus on the standard OTOC

$$F_{\text{OTO}}(t) \equiv \langle \hat{O}(t) \hat{O} \hat{O}(t) \hat{O} \rangle - \langle \hat{O}(t) \hat{O} \rangle^2 = F_c(t, 0, t, 0), \quad (\text{S14})$$

and the square commutator

$$c(t) \equiv - \left(\langle [\hat{O}(t), \hat{O}]^2 \rangle - \langle [\hat{O}(t), \hat{O}] \rangle^2 \right) \quad (\text{S15}) \\ = F_c(t, 0, 0, t) + F_c(0, t, t, 0) - 2\text{Re}F_c(t, 0, t, 0).$$

We now restrict our analysis with the assumption that the matrix elements in the ETH from Eq.(1) are uncor-

related Gaussian variables, i.e.

$$\overline{R_{\alpha\beta} R_{\gamma\delta}} = \delta_{\alpha\delta} \delta_{\beta\gamma} \quad (\text{S16a})$$

$$\begin{aligned} \overline{R_{\alpha\beta} R_{\beta\gamma} R_{\gamma\delta} R_{\delta\alpha}} &= \overline{R_{\alpha\beta} R_{\beta\gamma}} \overline{R_{\gamma\delta} R_{\delta\alpha}} \\ &+ \overline{R_{\alpha\beta} R_{\gamma\delta}} \overline{R_{\beta\gamma} R_{\delta\alpha}} \\ &+ \overline{R_{\alpha\beta} R_{\delta\alpha}} \overline{R_{\beta\gamma} R_{\gamma\delta}} . \end{aligned} \quad (\text{S16b})$$

This allows us to re-write the four point function Eq. (S13) evaluated over $\hat{\rho} = \sum_n p_n |E_n\rangle \langle E_n|$ as

$$F_c(t_1, t_2, t_3, t_4) = \sum_n p_n F_c(E_n, t_1, t_2, t_3, t_4) , \quad (\text{S17})$$

where $F_c(E_n, t_1, t_2, t_3, t_4)$ is the micro-canonical expectation value, i.e., (S13) computed over a single eigenstate $|E_n\rangle$. One can observe that the same result holds from a

$$F_c(t_1, t_2, t_3, t_4) = f_1(t_1, t_2, t_3, t_4) + c_1(t_2 - t_3) + c_2(t_1 - t_4, t_2 - t_3) , \quad (\text{S18})$$

with

$$\begin{aligned} f_1(t_1, t_2, t_3, t_4) &= O^2 [F_2(t_1 - t_3) + F_2(t_2 - t_4) + F_2(t_1 - t_4) + F_2(t_2 - t_3)] \\ &+ OO' [F_2'(t_1 - t_3) + F_2'(t_2 - t_4) + 2F_2'(t_2 - t_3)] + \frac{1}{2} OO'' [F_2''(t_1 - t_3) + F_2''(t_2 - t_4) + 2F_2''(t_2 - t_3)] , \end{aligned} \quad (\text{S19a})$$

$$c_1(t_2 - t_3) = O'^2 F_2''(t_2 - t_3) , \quad (\text{S19b})$$

$$c_2(t_1 - t_4, t_3 - t_2) = F_2(t_1 - t_4) F_2(t_2 - t_3) + F_2'(t_1 - t_4) \frac{\partial F_2(t_2 - t_3)}{\partial E} , \quad (\text{S19c})$$

with $F_2(t)$ defined in Eq. (S3), O , O' and O'' obtained from the diagonal expectation value of the operator \hat{O} and its first and second derivative with respect to energy evaluated at E_n .

The functions $F_2'(t)$ and $F_2''(t)$ can be written as

$$\begin{aligned} 2\text{Re}F_2'(t) &\equiv - \sum_{\beta \neq n} \omega_{n\beta} (e^{i\omega_{n\beta}t} + e^{-i\omega_{n\beta}t}) |f_{n\beta}|^2 e^{-S_{n\beta}} \\ &= - \frac{1}{2\pi} \int d\omega \omega S_{\hat{O}}(E_n, \omega) e^{i\omega t} , \end{aligned} \quad (\text{S20a})$$

$$\begin{aligned} 2\text{Re}F_2''(t) &\equiv \sum_{\beta \neq n} \omega_{n\beta}^2 (e^{i\omega_{n\beta}t} + e^{-i\omega_{n\beta}t}) |f_{n\beta}|^2 e^{-S_{n\beta}} \\ &= \frac{1}{2\pi} \int d\omega \omega^2 S_{\hat{O}}(E_n, \omega) e^{i\omega t} , \end{aligned} \quad (\text{S20b})$$

where in the second line of Eq. (S20) we have identified sums with integrals and expanded the entropy terms around energy E_n . The resulting $S_{\hat{O}}(E_n, \omega)$ is the symmetric response function which can be computed within ETH as stated in Eq. (S5). Note that f_1 and c_1 vanish for $O(E_n) = 0$ and do not contain information about the distribution of the $R_{n\beta}$ in the ETH.

To derive Eq. (S18), we first write down F_c in the energy eigenbasis and, after invoking the ETH in

purely out-of-equilibrium calculation, where the expectation value in Eq. (S13) is taken over an initial pure state $|\Psi\rangle$. In this case, the distribution of the p_n is given by the overlaps with the initial state $p_n = |\langle E_n | \Psi \rangle|^2$. Similar to the procedure undertaken in Sec. S3, one can show that if p_n is compatible with statistical mechanics — with average energy E and small variance $\delta E^2 / E^2 \sim 1/L$ — the leading term of Eq. (S13) is simply given by the single eigenstate expectation value. One can however expect finite size effects, as shown by the numerical data in Fig. 4 of the main text and in Fig. S9 below. In the following, we consider only the microcanonical single eigenstate four-point functions and omit E_n in the notations.

Using Eq. (S16), one can re-write the four-point function in Eq. (S13) directly in terms of the two-point functions from Eq. (S3) as

Eq. (1) and the Gaussian uncorrelated approximation in Eq. (S16), we express $O_\beta = O(E_\beta)$ as a Taylor expansion around the energy E_n at second order in frequencies $\omega_{n\beta}$. Then, upon substituting discrete sums with integrals, we expand the exponential of entropy terms as done before in Eqs. (S20), to obtain the final result in Eq. (S18).

Therefore, the OTOC and square-commutator can be directly written as combinations of f_1, c_1 and c_2 in Eqs. (S19) as

$$F_{\text{OTO}}(t) = f_1(t) + c_1(t) + c_2(t) \quad (\text{S21})$$

$$c(t) = 2[c_1(0) + c_2(0) - c_1(t) - c_2(t)] . \quad (\text{S22})$$

Within this approximation, the leading terms in the system size of the square-commutator and of the OTOC read

$$F_{\text{OTO}} = |F_2(t)|^2 + 2O(E_n)^2 \text{Re}[F_2(t) + F_2(0)] , \quad (\text{S23})$$

$$c(t) = 2|F_2(0)|^2 - 2|F_2(t)|^2 . \quad (\text{S24})$$

In fact, all the terms containing derivatives with respect to energy are proportional to $1/L$ and are therefore sub-leading in L with respect to $|F_2(t)|^2$, both for local or sums of local operators. Note, however, that these terms could be relevant in large- L chaotic models at intermediate times, where the square-commutator is expected

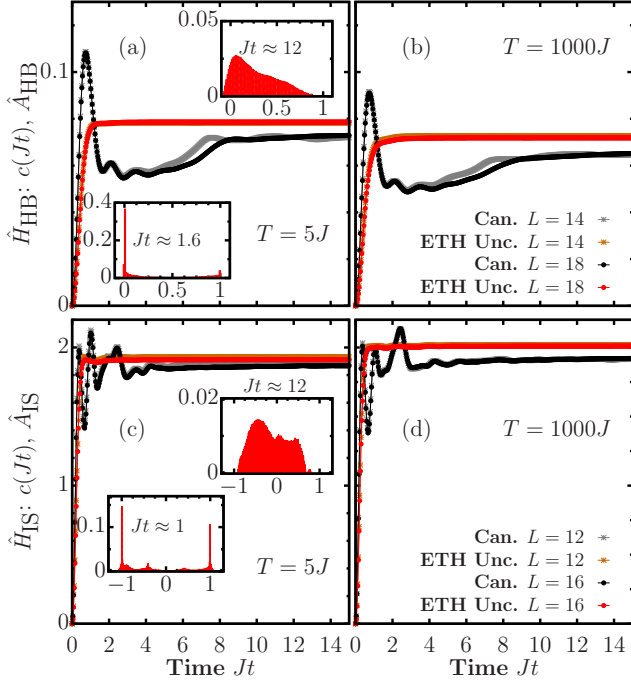


FIG. S9. Time-dependent square-commutator from Eq. (S15) for the operators \hat{A}_{HB} [(a),(b)] and \hat{A}_{IS} [(c),(d)] for \hat{H}_{HB} and \hat{H}_{IS} at temperatures $T = 5J$ [(a) and (c)] and $T = 1000J$ [(b) and (d)]. The expectation value obtained for a canonical state is compared with the one obtained assuming the ETH and uncorrelated R_{nm} for increasing system size L . Insets show the distribution of eigenvalues of the matrix $\hat{O}^{\omega_c=2\pi/t}$ [Eq. (6) of the main text] for the largest system size displayed in each case

to grow exponentially as $\sim e^{2\lambda t}/L^2$, with λ the classical Lyapunov exponent [51].

B. Numerical evaluation of the square-commutator

The square commutator as defined in Eq. (S15) can be directly evaluated from the ETH assuming uncorrelated

R_{nm} from Eq. (1) using the procedure described above. The resulting expression depends only on the dynamics of two-point functions which can be evaluated using the procedure described in Sec. S2. We have evaluated the resulting expression [Eq. (S22)] in our generic models \hat{H}_{HB} and \hat{H}_{IS} [Eqs. (2)-(3) of the main text] to compare against the corresponding square commutator evaluated in the canonical ensemble. For the specific case of local observables \hat{A} , the results are shown in Fig. S9, while for sums of local operators \hat{B} the results are shown in Fig. 4 of the main text.

The existence of a discrepancy between the dynamics of the square commutator computed in the canonical ensemble and the ETH assuming uncorrelated R_{nm} is apparent in the short-intermediate timescales in Fig. S9. This indicates that, unlike the dynamics of two-point functions in Sec. S2, the correlations associated to the distribution of R_{nm} are only significant for higher order correlation functions. In the long-time regime, however, it appears that the emerging GOE statistics at short frequencies implies that the degree of correlations are irrelevant to the underlying long-time dynamics. The saturation value predicted from the ETH assuming R_{nm} are uncorrelated approximately converges to the one obtained in the canonical ensemble. This saturation value is better approximated as the system size is increased as observed in Fig. 4 of the main text. From Fig. S9, however, the convergence in the long-time value is less apparent at the system sizes L we have access to. As discussed in the main text, the data is consistent with a saturation time related to the frequency ω_{GOE} by $t_s \approx 2\pi/\omega_{\text{GOE}}$. The insets in Fig. S9 describe the degree of correlations relevant to the dynamics at two different points in time for the largest system size displayed. The eigenvalue distribution for $\hat{O}^{\omega_c=2\pi/t}$ strongly deviates from the GOE behaviour at the (large) ω_c frequencies relevant to the short-time dynamics. As the ω_c value is decreased, the degree of correlations seem to decrease as well, just as the square commutator approaches saturation. As stated in the main text, this behaviour indicates that the OTOC's encode the statistical properties of R_{nm} from Eq. (1).